Preprints.org

Article

WindRAD Scatterometer Quality Control in Rain

Zhen Li [*] , Anton Verhoef , Ad Stoffelen

Article

WindRAD Scatterometer Quality Control in Rain

Zhen Li *,†, [ID] **, Anton Verhoef** †[ID] **and Ad Stoffelen** †,[ID]

Royal Netherlands Meteorological Institute

* Correspondence: zhen.li@knmi.nl
† Current address: Utrechtseweg 297, 3731 GA De Bilt, the Netherlands.

Abstract: Rain backscatter corrupts Ku-band scatterometer wind retrieval by mixing with the signatures of the backscatter measurements (σ°) on the sea surface. The measurements are sensitive to rain clouds due to the short wavelength, and the rain-contaminated measurements in a WVC (Wind Vector Cell) deviate from the measurements that are simulated using the wind GMF (Geophysical Model Function). Therefore, QC (Quality Control) is essential to guarantee the retrieved winds' quality and consistency. The normalized MLE (Maximum Likelihood Estimator) residual (R_n) is a QC indicator representing the distance between the measurements and the wind GMF; it works locally for one WVC. J_{OSS} is another QC indicator. It is the speed component of the observation cost function, which is sensitive to spatial inconsistencies in the wind field. $R_n J$ is a combined indicator, and it takes both local information (R_n) and spatial consistency (J_{OSS}) into account. This paper focuses on WindRAD on the FY-3E (Fengyun-3E) satellite, a dual-frequency (C and Ku band) rotating-fan-beam scatterometer. The R_n and $R_n J$ have been established and thoroughly investigated for Ku-band-only and combined C&Ku wind retrieval. A polynomial fit is applied to select the optimal R_n threshold. The C-band measurements are hardly influenced by rain, so the Ku-based R_n is proposed for the C&Ku wind retrieval instead of the total R_n from both C and Ku bands. In conclusion, the $R_n J$ gives the optimal QC result for the Ku-band-only and C&Ku wind retrieval. Adding the C-band into the retrieval suppresses the rain effect; therefore, a promising QC skill can be achieved with fewer rejected winds.

Keywords: WindRAD; dual frequency wind scatterometer; rain contamination; quality control; wind retrieval; rotating-fan-beam

---

1. Introduction

FY-3E (Fengyun-3E) is one of the Chinese FY-3 meteorological satellite series, it was launched on 5 July 2021. It carries the WindRAD (Wind Radar) scatterometer, the first dual-frequency (C and Ku band) rotating-fan-beam scatterometer. The number of normalized radar cross sections (the backscattered power from the wind-roughed sea surface, called σ°s) increases significantly as compared to the rotating-pencil-beam (e.g., HY-2B / C / D (Hai Yang) [1]) and the fixed-fan-beam (e.g., ASCAT-B / C (Advanced Scatterometer) on Metop [2]) instruments, due to the dual-frequency rotating-fan-beam design. The characteristics of the geometries and the σ° measurements have been discussed in [3], and an improved calibration method designed for WindRAD was introduced in [4]. This paper focuses on the QC (Quality Control) for rain contamination in the Ku-band involved wind retrievals.

WindRAD level-1 data are organized in WVCs (Wind Vector Cells), a sub-track coordinate system with axes oriented along and across the swath. The scatterometer retrieves wind in each WVC from σ°s. The σ°s, associated with their respective geometries (azimuth angle, incidence angle, frequency, and polarization), are inverted through a GMF (Geophysical Model Function) with the MLE (Maximal Likelihood Estimation) method to derive the winds [5–9].

Scatterometer winds are operationally used for nowcasting, assimilated into NWP (Numerical Weather Prediction) models and they are used in many oceanographic and climate studies [10–14]. Therefore, QC is essential to guarantee the quality and consistency of the retrieved winds in these applications. Raindrops are relatively small compared to the radar wavelength, which can cause Rayleigh volume scattering in the atmosphere. The Rayleigh scattering effect is inversely proportional to the fourth power of the wavelength. Larger raindrops and smaller wavelengths lead to more intense

Rayleigh scattering. Therefore, Ku-band observations are much more sensitive and are about 40 times more affected by rain than C-band observations [15–18]. Consequently, the backscatter signal σ° is generally enhanced, and the rain enhancement effect disturbs the Ku-band wind retrievals [19–21]. The rain-induced backscatter is generally larger than the wind-induced backscatter, which leads to positively biased retrieved winds up to 15 m/s. The substantial biases under moderate and heavy rain result in poor retrieval performance; therefore, these WVCs must be identified and flagged.

Several rain QC methods have been developed for Ku-band scatterometers. The normalized MLE residual (R_n) is the most common QC indicator, which has been implemented on all pencil-beam scatterometers and the CFOSAT rotating fan-beam scatterometer [16,22–24]. It indicates how well the σ° measurements fit the wind GMF in one WVC. Rain backscatter is isotropic and causes a deviation of the measured σ°s from the wind GMF σ°s. Thus, the R_n is larger than it is under dry weather conditions. Another indicator is J_{OSS}, it uses the speed component of the observation cost function in the 2DVAR (2-D Variational Ambiguity Removal) ambiguity removal step to accept extra WVCs which are rejected by the R_n indicator [17,25]. A rain GMF was introduced in [18] based on Bayesian retrieval and utilizing the Ku-band sensitivity at HH and VV polarization to the rain (rain GMF).

This article proposes a combined QC method with R_n and J_{OSS} called R_nJ for Ku-band-only and C&Ku wind retrieval. Section 2 describes the used datasets and briefly summarizes the R_n and the J_{OSS} QC algorithms and their adaptation for WindRAD data. The Ku-band-only and C&Ku wind retrieval with R_n and R_nJ QC methods are analyzed and discussed in Section 3 and Section 4. It is the first time to investigate the QC for the C&Ku combined wind retrieval. The C-band is not sensitive to rain; therefore, by adding the C-band in wind retrieval, the contribution of the Ku-band in R_n is more discriminating for QC than the total R_n of C&Ku. Thus, the Ku-based R_n is proposed as a quality indicator. It is discussed in Section 4. The conclusion is given in Section 5.

2. Data and QC Algorithms

2.1. WindRAD Data

The operational WindRAD data version has been updated in May 2023. Level-1 data are organized in WVCs with a size of 20 km × 20 km or 10 km × 10 km. Each WVC contains σ°s in C-band at 5.40 GHz and in Ku-band at 13.256 GHz with horizontal (HH) and vertical (VV) polarizations. The incidence angles range between 33.0° and 44.0° for C-band, and between 36.5° and 44.0° for Ku-band. The characteristics of the WindRAD data have been described in [3].

In this article, we use the 20 km level-2 updated operational version BUFR (Binary Universal Form of Representation meteorological data) products, which is internal OSI SAF (Ocean and Sea Ice Satellite Application Facility) data produced at KNMI (Royal Netherlands Meteorological Institute). The data set runs from Aug to Oct 2023 (ascending orbits) for the QC algorithm adaption and we use longer term data from Aug 2023 to March 2024 (ascending orbits) for the algorithm validation. For descending orbits, the parameters of the QC algorithms investigated in this paper were adjusted, while the methodology is general and applicable along the whole orbit. The QC results show the same effectiveness on ascending and descending orbits; thus, the descending orbits are not shown here. The level-2 products are retrieved with the CMOD7 GMF for C-band and NSCAT-4DS GMF for Ku-band (SST (Sea Surface Temperature) effect is eliminated). The C-band σ°s are calibrated with HOC (Higher Order Calibration) and NOCant (NWP Ocean Calibration as a function of incidence angle and relative antenna angle). The Ku-band σ°s are calibrated with NOCant [4].

2.2. 3IMERG Precipitation Product

The 3IMERG (level-3 Integrated Multi-satellitE Retrievals for GPM) precipitation product utilizes information from the GPM (Global Precipitation Measurement) satellite constellation to estimate precipitation over the majority of Earth's surface. The algorithm of 3IMERG products intercalibrates, merges, and interpolates multiple satellite microwave precipitation estimates, as well as microwave-calibrated infrared satellite estimates and precipitation gauge analyses. The system first gives a quick

estimate, called IMERG Early Run, and later on a better estimate, when more data are included (IMERG Late Run). In the end, roughly 3.5 months after acquisition time, a research level product including monthly gauge data is provided called IMERG Final Run. In this article, the IMERG Final Run V07 product is used [26]. The instantaneous microwave-only precipitation estimate is applied for better consistency with the scatterometer wind products. The chosen precipitation product is called GPM data hereafter.

The GPM product has a spatial resolution of $0.1°$ and a time resolution of 30 min, covering the latitude range of -60° to 60°. Thus the rain grid is smaller than a WVC (20 km). All the rain grid points overlapping a WVC are taken into account with weighted averaging. The time difference between the GPM data and the scatterometer data is limited to less than 15 min.

2.3. NWP Wind

NWP winds from the ECMWF (European Centre for Medium-Range Weather Forecasts) operational forecast model are used. Hourly forecasts with time steps of +3 h, +4 h, ..., and +21 h are available. The model winds have been interpolated in space and time to the WVCs. The equivalent neutral 10-m winds have been converted to stress-equivalent 10-m winds, correcting for the effect of air mass density [27]. Model winds are available at every scatterometer WVC, and their spatial representativeness and high quality have been investigated in detail in [28], with a careful error assessment of scatterometer winds, in-situ winds, and ECMWF model stress-equivalent winds.

2.4. R_n QC Algorithm

The QC indicator R_n, or normalized MLE residual, has been widely used for Ku-band scatterometers as described in Section 1. The MLE is defined for each WVC as [5–9]:

$$MLE = \frac{1}{N} \sum_{i=1}^{N} (\frac{\sigma_{mi}^° - \sigma_{si}^°}{K_p(\sigma_{mi}^°)})^2,\tag{1}$$

where N is the number of views in a WVC, $\sigma_{mi}^°$ is the backscatter measurement, $\sigma_{si}^°$ is the simulated backscatter through the GMF, and $K_p(\sigma_{mi}^°)$ is the measurement error variance. The MLE is defined as the distance between a set of measured $\sigma°$s and simulated $\sigma°$s that lie on the wind GMF manifold in an N-dimensional space. The normalized MLE residual is defined as $R_n = MLE/\langle MLE \rangle$. $\langle MLE \rangle$ is the expected MLE in a particular WVC across the swath and for a specific wind speed. Thus, R_n is a function of WVC number and wind speed [16].

The algorithm needs to be adapted for WindRAD data. Firstly, the number of views for a pencil-beam scatterometer is always four for all WVCs across the swath; however, this number varies for the WindRAD rotating-fan-beam scatterometer [3]. Therefore, before calculating $\langle MLE \rangle$, the MLE must be normalized by the number of views in a particular WVC. Secondly, the shape of the threshold is set differently. In [16], the R_n threshold is defined by following the contour line of the R_n as a function of wind speed. It is defined as a parabolic line for lower wind speeds, combined with a straight line for wind speeds above 15 m/s. However, the WindRAD contour lines of the R_n are different mainly because the number of views for a WVC is much more than four. Figure 1 is an example of the R_n contour plot (Ku-band). The contour lines are more like a Gaussian distribution than like a parabolic distribution. Thus, a polynomial fit is applied to define the threshold. We still define the threshold as a constant value at wind speeds above 15 m/s, because otherwise more and more data are rejected with increasing wind speed until all the high winds are rejected. The threshold at a wind speed lower than 5 m/s is also set to a straight line since rain generally does not result in low wind speed retrievals. WVCs with R_n higher than the threshold are considered contaminated with rain and flagged. In Sections 3.1 and 4.1, we give the evaluation of the threshold experiments for the Ku-band and C&Ku band.
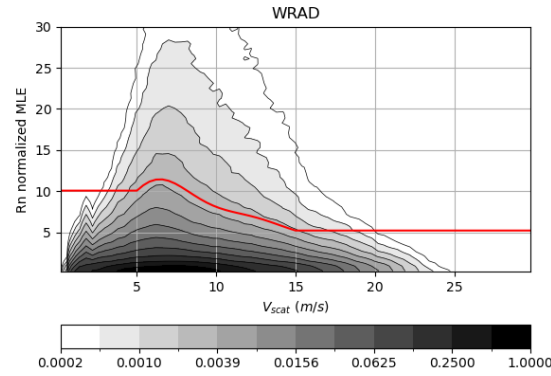
Figure 1. Ku-band two dimensinal histogram of R_n as a function of the NWP wind speed (data Aug 2023 to Oct 2023). The gray scale shows the fractional number of WVCs per R_n and wind speed bin. The red line is the example threshold for the R_n.

2.5. J_{OSS} QC Algorithm and Its Adaption to $R_n J$

Xu and Stoffelen [17] proposed J_{OSS} as a QC indicator in addition to R_n for pencil-beam scatterometers. This method has also shown its capability for the rotating fan-beam scatterometer CFOSAT [25]. In the wind retrieval ambiguity removal (2DVAR) step, a wind field is constructed from the scatterometer wind ambiguities and the NWP winds by minimizing a cost function with constraints on meteorological consistency, which is called the analysis wind field [29]. J_{OSS} is defined as

$$J_{OSS} = f - f_S, \tag{2}$$

where f is the analysis wind speed derived in 2DVAR and f_S is the selected retrieved wind speed. In the previous study [17], the R_n QC for the pencil-beam scatterometer appeared to be too conservative with a high rejection rate (5 - 6%), and J_{OSS} was used to accept extra WVCs that were rejected by R_n. J_{OSS} is an excellent complementary indicator. For WindRAD, a proper R_n threshold will be set first. Then J_{OSS} is used to flag additional rainy WVCs, not detected by R_n. In this way, the local information (R_n) and spatial consistency (J_{OSS}) are both taken into account. The WVCs with J_{OSS} value lower than a certain threshold are considered rain-contaminated. The threshold value was modeled by three straight lines as a function of the wind speed [30], which also performs well on WindRAD data (see Section 3.2):

$$J_{OSS} = \begin{cases} 0.3 \times v - 4.2 & \text{if } v < 9m/s \\ -1.5 & \text{if } 9m/s \le v < 18m/s \\ -0.4 \times v + 5.7 & \text{if } v > 18m/s \end{cases} \tag{3}$$

3. Ku-Band R_n and $R_n J$ QC Results and Discussion

3.1. R_n QC Evaluation

The critical point of the R_n QC method described in Section 2.4 is to set an appropriate threshold. The threshold is a trade-off between the data rejection of all rain-contaminated WVCs and the data rejection of good wind retrievals. WindRAD data from Aug to Oct 2023 (more than 37 million WVCs) are used to calculate the R_n distribution. Various experiments are performed to find the optimal trade-off for the threshold. Figure 2 shows the selected tested thresholds from low rejection rate to high rejection rate: V1 (version 1, blue), V2 (version 2, green), and V3 (version 3, red).
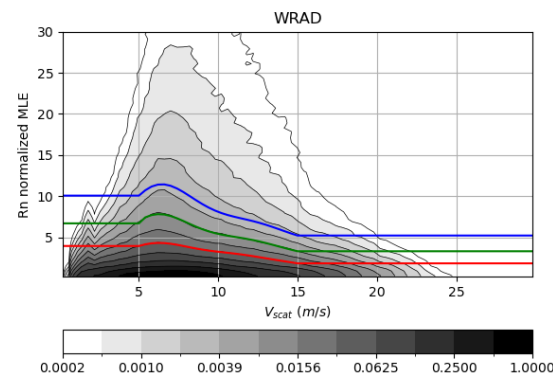
Figure 2. R_n contour plot with the wind solution closest to the ECWMF wind at different threshold: blue line V1; green line V2; red line V3 (see text), the gray scale shows the fractional number of WVCs.

Data from Aug 2023 in the latitude band between -20° and 20°, focusing on tropical moist convection processes, are used to evaluate the experiments. Figure 3 a, b, c show the tropical geographical distribution of the rejected winds for V1, V2, and V3, having rejection rates of 1.64%, 2.42%, and 5.44% respectively. The lower the rejection rate, the worse the rejected wind speed statistics are (Figure 3 f, e, d), since R_n QC starts to reject wind from the WVCs with the highest R_n value (the most likely being rain contaminated) until it reaches the threshold. The rejected winds with the lowest rejection rate contain the least good quality winds. Hence, they have the worst wind statistics (V1). On the other hand, a low rejection rate allows more rain-contaminated WVCs winds to be accepted. Figure 4 a and b show the V1 R_n accepted winds collocated with the rain rate, and the V1 R_n accepted winds collocated only with rain rates above 7 mm/hr. Most of the winds with high rain rates are excluded from the accepted winds, but compared with V2 and V3 (Figure 4 c - f), the collocated rain rates of the accepted winds (left panel) for V1 are the highest, and more high rain rate (above 7 mm/hr) winds are accepted. V3 has the smallest number of WVCs with a rain rate higher than 7 mm/hr and the lowest rain rates for the accepted winds. But the rejected winds scatter plot (Figure 3 f) shows that the core (the darkest red part of the contour) is closest to the diagonal. In contrast, the cores of V1 and V2 (Figure 3 d and e) are further away from the diagonal, with a larger retrieved wind speed bias caused by rain. This indicates that too many good quality winds (along the diagonal) are rejected with V3 QC. Later on, in Section 3.2, the J_{OSS} method will be combined with R_n to exclude additional rain-contaminated WVCs, thus, V3 R_n is too strict. In conclusion, V1 rejects too few WVCs and keeps more rain-contaminated WVCs as accepted winds. V3 rejects more WVCs which still contain relative good quality winds. Hence, V2 R_n is the optimal trade-off between the maximum rejection of low-quality data and the minimum rejection of high-quality data.
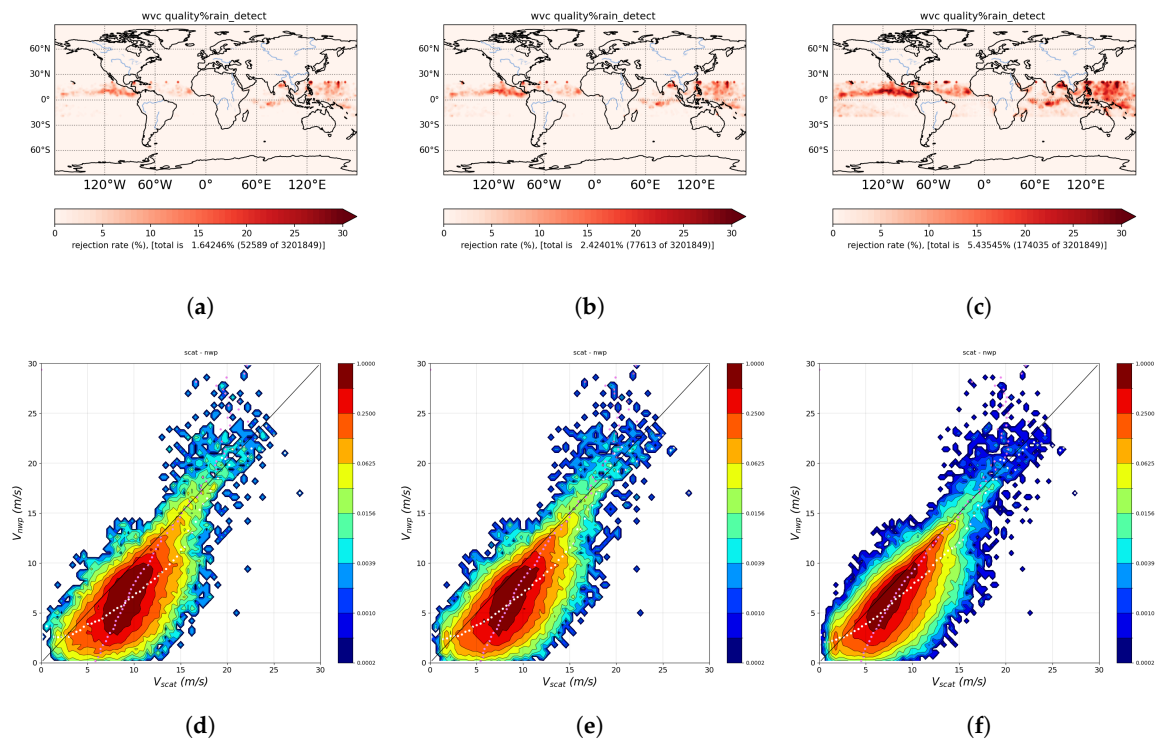
Figure 3. Rejected winds distribution within latitude [-20, 20] and their corresponding wind speed contour plots (retrieved winds versus NWP winds) for different R_n thresholds: V1 (**a, d**), V2 (**b, e**), V3 (**c, f**). In (**d, e, f**), the white dotted line shows the average wind speed of the NWP wind per retrieved wind, the light purple dotted line shows the average wind speed of the retrieved wind per NWP wind.
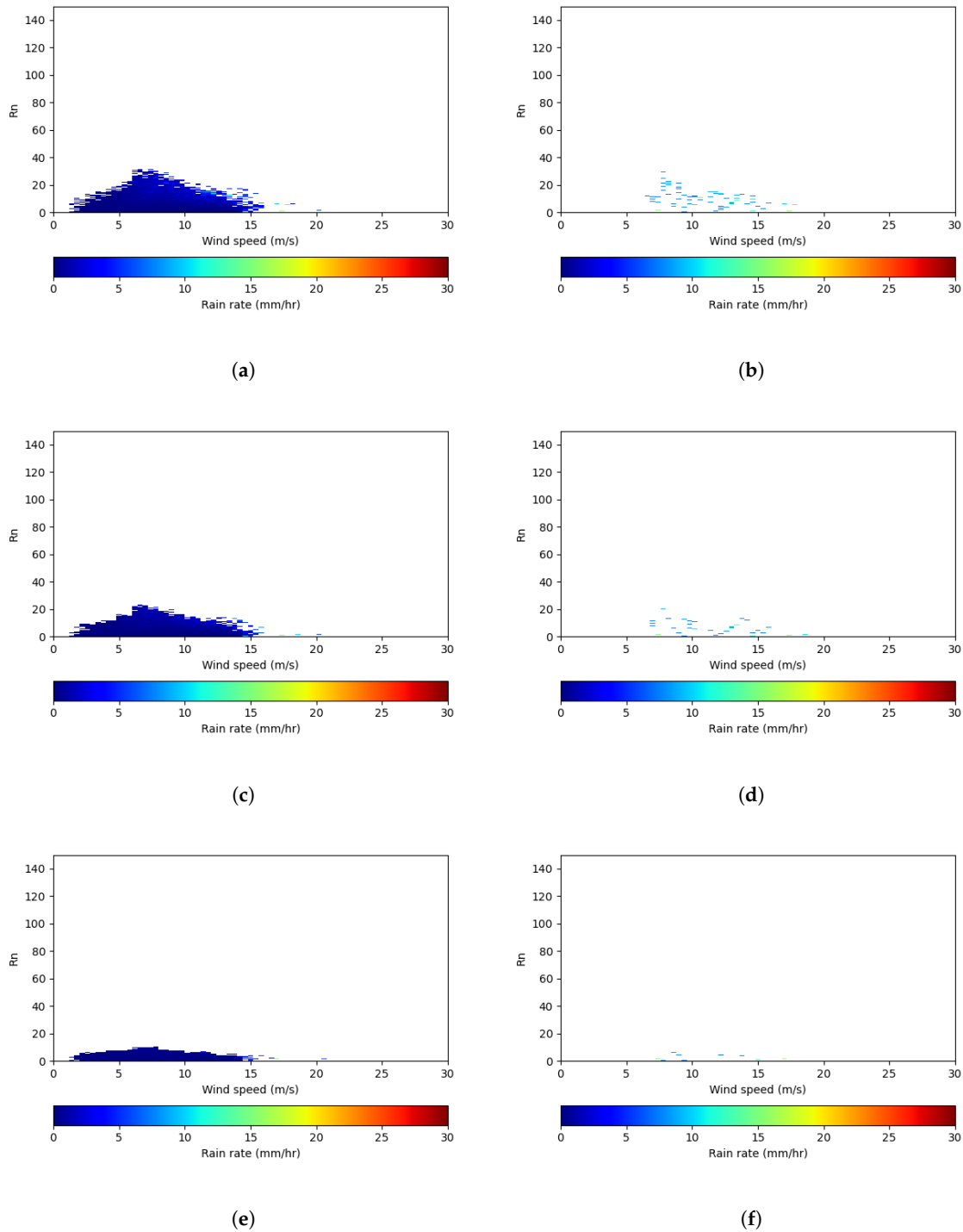
Figure 4. Left panels: R_n versus accepted retrieved wind speed, collocated with rain rate. Right panels: R_n versus the accepted retrieved wind speed for rain rates above 7 mm/hr. (**a, b**) R_n V1, (**c, d**) R_n V2, (**e, f**) R_n V3.

A long-term dataset from Aug 2023 to March 2024 validates the selected R_n QC (Figure 5). The rejection rate of the tropical region is 2.46%, and the wind speed contour plot against the NWP wind shows a similar result as in August 2023 only. The accepted winds with a rain rate above 7 mm/hr are 0.014% of the total accepted winds, about half the fraction obtained from the V1 R_n QC (0.026%). C-band wind retrievals are little influenced by rain and can be compared with the Ku-band winds. Thus,

the Ku-band rejected winds are compared with the collocated accepted C-band winds from WindRAD. The rejected winds have a notable deviation from the C-band winds because rain contamination increases the backscatter, leading to a false large wind retrieval result (Figure 6 a). The wind speed PDF (Probability Density Function) of the rejected winds (Figure 6 b) is compared to the PDF of the corresponding accepted C-band winds, which is in agreement with Figure 6 a. The V2 R_n QC is also applied globally (except for the polar regions to avoid sea ice contamination) with a rejection rate of 3.58% (Figure 7), and the accepted winds with rain rate above 7 mm/hr are about 0.013% of the total number of accepted winds, which is similar to the tropical region. The long-term dataset hence validates the suitability of the chosen V2 R_n QC threshold.
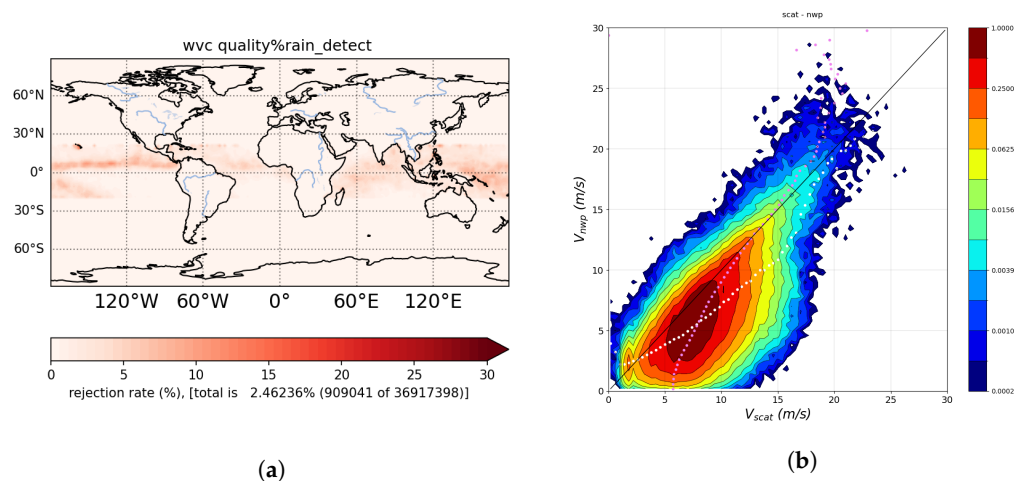

(**a**)   (**b**)

Figure 5. Long term (Aug 2023 to March 2024) V2 R_n QC rejected winds geographical distribution within latitutde [-20°, 20°]) (**a**) and its corresponding wind speed contour against NWP winds (**b**).

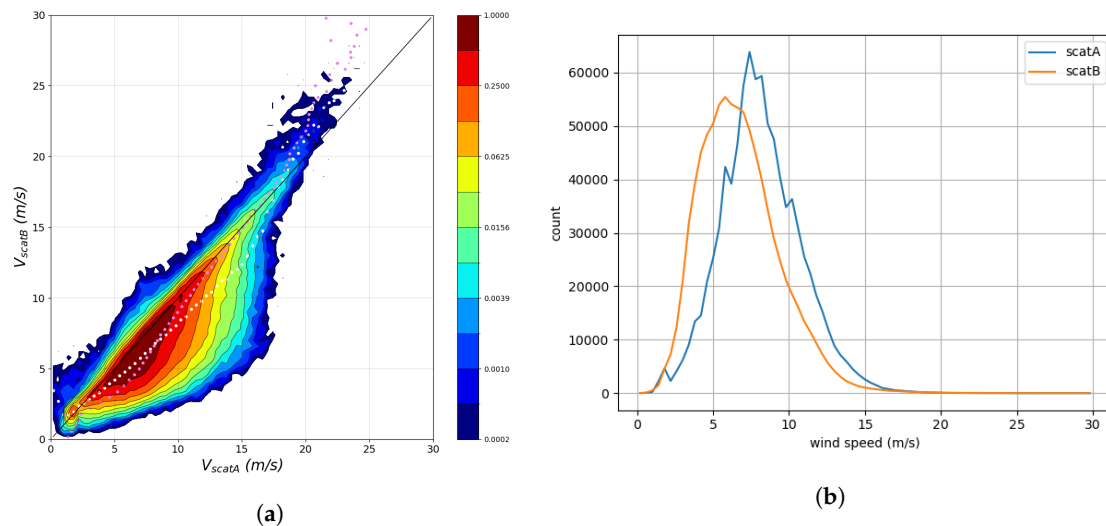(**a**)   (**b**)

Figure 6. Long-term statistics from Aug 2023 to March 2024 for tropical region (latitude [-20°, 20°]) between the rejected winds from Ku-band WindRAD V2 R_n QC (scatA) and the collocated accepted winds from C-band WindRAD (scatB): (**a**) the contour plot of rejected winds (Ku) vs. accepted winds (C), the color bar shows the fractional number of WVCs; (**b**): the wind speed PDF of rejected winds (Ku-band) and accepted winds (C-band).
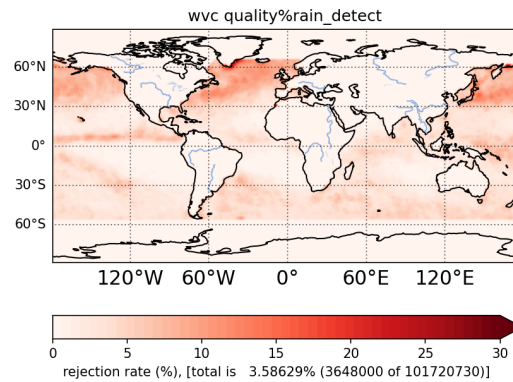
Figure 7. Long-term (from Aug 2023 to March 2024) geographical distribution of rejected winds for V2 R_n QC, latitudes between [-55°, 60°].

3.2. $R_n J$ QC Evaluation

The R_n threshold has been determined in Section 3.1, together with the J_{OSS} threshold (eq. 3). In the combined method $R_n J$, a WVC is rejected when its R_n higher than the R_n threshold or its J_{OSS} is lower than the J_{OSS} threshold. $R_n J$ includes both the rain local effect in an individual WVC (R_n) and the spatial inconsistency caused by rain (J_{OSS}). In this section, data from Aug 2023 to March 2024 are used.

Figure 8 shows the J_{OSS} collocated with rain as a function of the analysis wind field constructed in the wind retrieval 2DVAR step (see Section 2.5). The WVCs with a J_{OSS} value lower than the threshold (the red line in Figure 8) are flagged, and they are indeed associated with high rain rates. Figure 9 shows the geographical distribution of the rejected winds by R_n and J_{OSS} in the tropics, the rejection rates are 2.46% and 1.18%, respectively. The total rejection rate of $R_n J$ is 2.87%. This is lower than the sum of the two rejection rates, since there is some overlap between the two QC methods. An additional 0.41% of all WVCs are rejected by $R_n J$ as compared to R_n. If the statistics of the rejected winds become worse with more rejected winds, and at the same time, the statistics of the accepted winds become better or stay very similar, then, this confirms that the more rejected winds are low quality and presumably rain-contaminated, which means $R_n J$ is more effective. Table 1 and Table 2 show the wind statistics of the rejected winds and the accepted winds compared to the NWP winds and the WindRAD C-band winds, respectively. The statistics of the $R_n J$ accepted winds vs. the NWP winds are generally slightly better than the R_n winds. The rejected winds' speed bias and the SDD of the u v components vs. the NWP winds are all become worse with $R_n J$ than with R_n. Similarly, the statistics of the $R_n J$ accepted winds against the WindRAD C-band are all slightly better than the accepted winds by R_n, and the statistics of the rejected winds by $R_n J$ are either worse or stay very similar to the rejected winds by R_n.
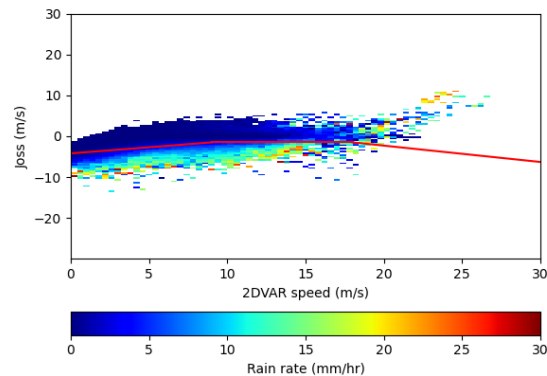
Figure 8. Ku-band J_{OSS} value collocated with rain as a function of the analysis wind speed wind speed. The red line is the threshold mentioned in eq. 3. Data are from Aug 2023 to March 2024, latitude [-20°, 20°].
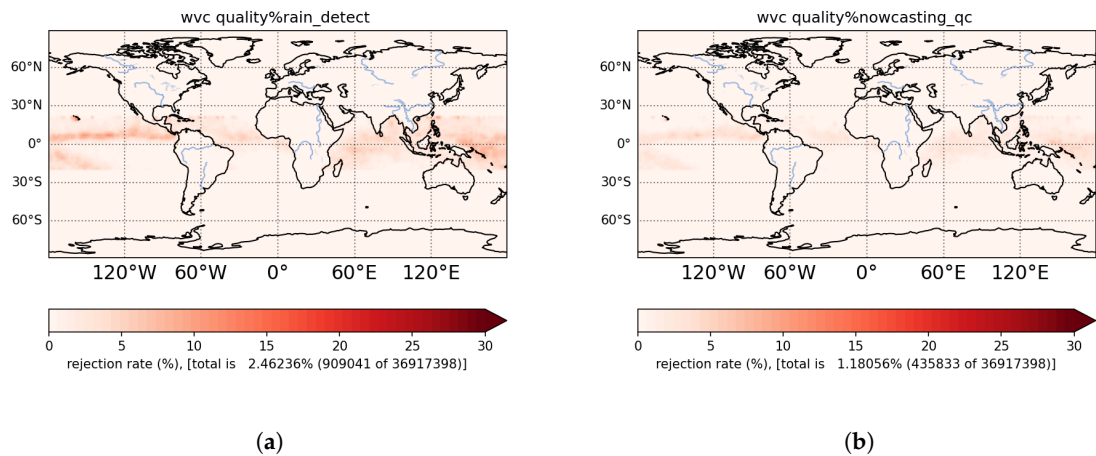

(**a**)   (**b**)

Figure 9. Geographical distribution of the rejected winds for the data from Aug 2023 to March 2024, latitude [-20°, 20°]: (**a**) the winds rejected by R_n QC; (**b**) the winds rejected by J_{OSS} QC.

Table 1. Ku-band wind statistics comparison of R_n and R_nJ against NWP winds, tropical region latitude [-20°, 20°], data from August 2023 to March 2024.

	QC method	Speed bias (m/s)	SDD of u (m/s)	SDD of v (m/s)
Rejected winds	R_n	2.312	2.34	2.38
	R_nJ	2.491	2.39	2.44
Accepted Winds	R_n	0.113	1.15	1.19
	R_nJ	0.096	1.13	1.17

Table 2. Ku-band wind statistics comparison of R_n and R_nJ against WindRAD C-band winds, tropical region latitude [-20°, 20°], data from August 2023 to March 2024.

	QC method	Speed bias (m/s)	SDD of u (m/s)	SDD of v (m/s)
Rejected winds	R_n	1.469	2.99	2.42
	R_nJ	1.466	3.09	2.53
Accepted Winds	R_n	0.367	1.34	1.29
	R_nJ	0.362	1.32	1.28

$R_n J$ rejects only 0.41% extra winds as compared to R_n. However, $R_n J$ still has a positive impact on the accepted wind statistics, and the statistics of the rejected winds by $R_n J$ are either worse than R_n or stay similar. Additionally, $R_n J$ accepts only 0.007% of the winds with a rain rate above 7 mm/hr, this is half the amount which is accepted by R_n (0.014%). Therefore, $R_n J$ has a better capability to filter rain-contaminated WVCs than R_n.

4. C&Ku Combined R_n and $R_n J$ QC Results and Discussion

4.1. Evaluation of the Ku Contribution to R_n on QC

The MLE of the C&Ku wind retrieval includes both C and Ku frequencies (eq. 1). However, the C-band measurements are only little influenced by rain; therefore, the contribution of the C-band R_n, due to measurement noise, can dilute the effect of rain on the MLE and it may not be accurate to use the total R_n, based on both C- and Ku-band inputs, to set the QC threshold. Figure 10 (a and b) shows the total R_n and the Ku-based R_n. We first discuss the respective QC results and assess the advantage of using only the Ku-based R_n, and then investigate the optimal threshold for R_n.
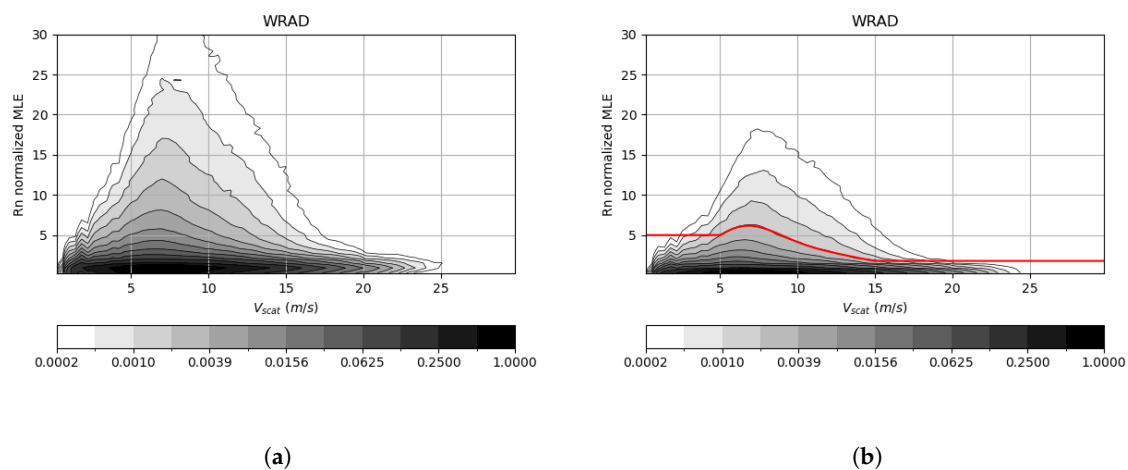

| (a) | (b) |

Figure 10. R_n contour plot of the C&Ku wind solution closest to the NWP winds, the color bar shows the fraction of WVC numbers: (**a**) the total R_n; (**b**) the Ku contribution to R_n, the red line shows the optimal threshold (see text).

Data from August to October 2023 with latitudes between -20° and 20° are used. A similar amount of rejected winds is required to equally compare the rejected wind statistics between the use of total R_n and the Ku-based R_n. As shown in Section 3.1, the R_n QC starts to reject the winds with the highest R_n value, these are most likely rain-contaminated. So, a low rejection rate (lower than 1%) is chosen to ensure that the rejected winds contain a minimal number of good quality winds. Figures 11 a and b show the geographical distribution of the rejected winds in the tropical region for the total R_n and the Ku-based R_n, with a rejection rate of about 0.7% for both. Against the NWP winds, the rejected wind speed of the Ku-based R_n (Figure 11 d) shows a significantly larger deviation from the diagonal compared to the rejected winds using the total R_n (Figure 11 c). Therefore, with the same amount of rejected winds, the Ku-based R_n can more accurately identify the rain-contaminated WVCs than the total R_n. The optimal QC threshold should be obtained from the Ku-based R_n.
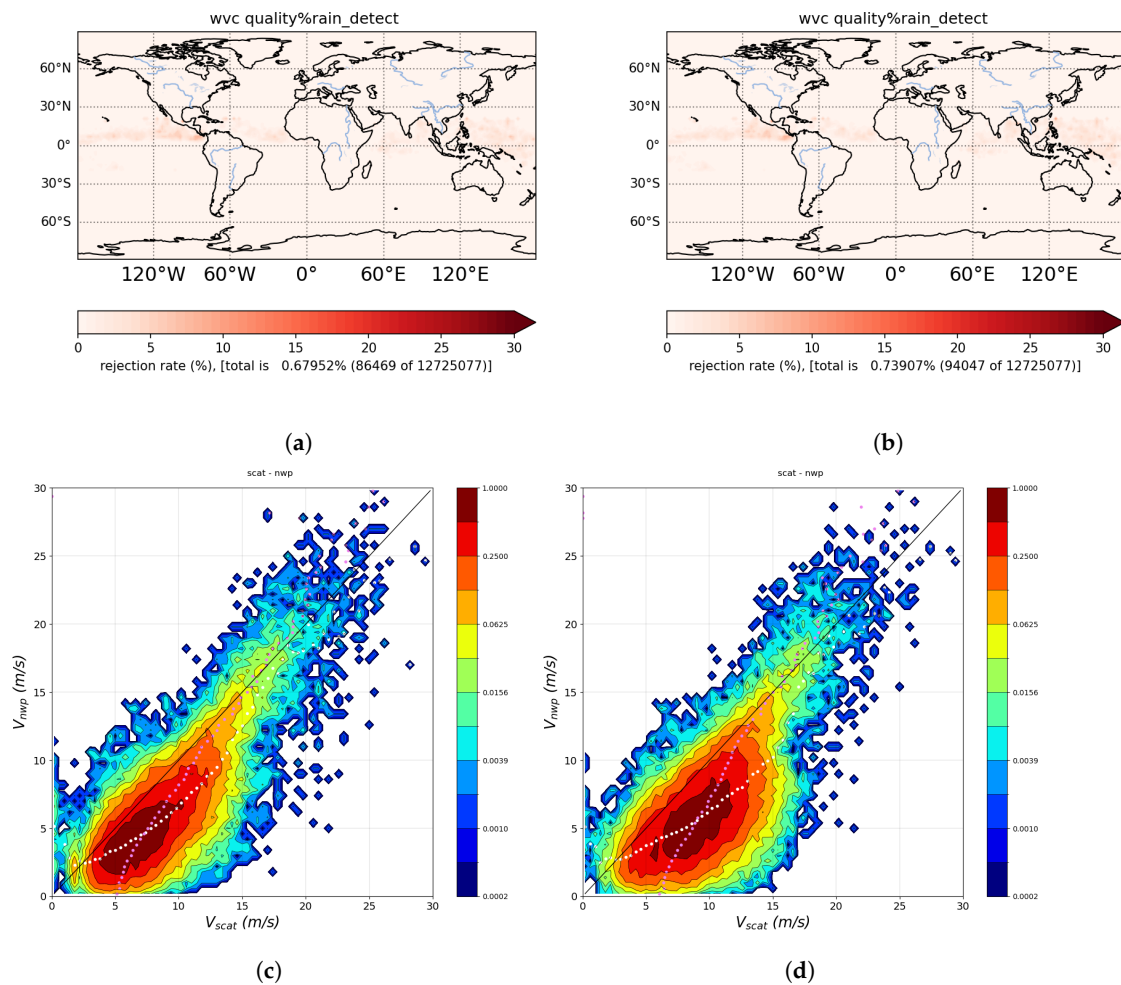
Figure 11. Top panels: geographical distribution of the rejected winds in the tropics $[-20°, 20°]$: (**a**) using the total R_n, (**b**) using the Ku-based R_n. Bottom panels: the rejected wind speed contour plot against NWP wind: (**c**) using the total R_n, (**d**) using the Ku-based R_n.

Various experiments like those described in Section 3.1 have been performed to select the optimal threshold (not shown). The chosen threshold is shown in Figure 10 b, it is a good trade-off between keeping as much as possible the good quality winds and rejecting as much as possible the rainy WVCs. The rejection rate calculated with data from August 2023 to March 2024 is 1.11% in the tropical region, about half of the rejection rate for Ku-band-only (2.46%). At the same time and with this reduced rejection rate, the rejected and accepted wind statistics against the NWP winds and the C-band WindRAD winds (Table 3) do not show a large difference compared to those of the Ku-band-only (Tables 1 and 2). In addition, the percentage of the accepted winds with a rain rate above 7 mm/hr is 0.041%, which is three times as much as when the Ku-band R_n is used (0.014%). This indicates that by adding C-band measurements to the wind retrieval, the rain effect is suppressed, and some of the WVCs rejected by Ku-band R_n are now accepted by C&Ku. Thus, the C&Ku wind retrieval can achieve similar QC results in terms of rejected and accepted wind statistics and still reject fewer WVCs. Hence, the C-band has a clear added value in rainy conditions to obtain improved vector winds.

Table 3. Rejected and accepted wind statistics (C&Ku) against NWP winds and against C-band WindRAD winds using the Ku-based R_n, data from August 2023 to March 2024.

	Compare against	Speed bias (m/s)	SDD of u (m/s)	SDD of v (m/s)
Rejected winds	NWP winds	2.301	2.24	2.35
	C-band (WindRAD)	1.375	2.28	2.40
Accepted Winds	NWP winds	0.120	1.14	1.22
	C-band (WindRAD)	0.359	1.27	1.22

4.2. $R_n J$ QC Evaluation

The combined QC method $R_n J$ is also applied on the C&Ku wind retrieval with the same procedure as in Section 3.2. The data from Aug 2023 to March 2024 are evaluated in the tropical region with latitudes between [-20°, 20°].

The rejection rate using J_{OSS} QC is 0.73%, the rejection rate using R_n QC is 1.11%, and the rejection rate using $R_n J$ QC is 1.53%. Hence, 0.42% of extra data are rejected using $R_n J$ as compared to R_n, which is almost the same number as for the Ku-band retrievals (0.41%). Figure 12 shows the speed contour plot of the rejected winds against NWP winds using R_n (a) and $R_n J$ (b). The rejected winds from $R_n J$ QC deviate more from the diagonal than the rejected winds from R_n QC. The statistics of rejected winds for $R_n J$ against NWP winds and the WindRAD C-band winds (Tables 4 and 5) are all worse than for R_n, except the wind speed bias against the WindRAD C-band winds is slightly better (very similar), which might be because the C&Ku winds contain the same C-band source. The accepted wind statistics for $R_n J$ QC are all slightly better than the accepted wind statistics for R_n QC (Tables 4 and 5). As described in Section 3.2, only when the extra rejected winds are rain-contaminated (low quality), the statistics of the rejected winds will become worse with more rejected winds, whereas the statistics of the accepted winds will become better or stay similar. Therefore, as discussed above, the extra rejected winds by $R_n J$ are rain-contaminated and which is not detected by R_n. Furthermore, the accepted winds with rain rates above 7 mm/hr are about 0.027% of the total wind count, a reduction of more than one-third as compared to R_n QC (0.041%). In conclusion, the $R_n J$ can further identify the rain-contaminated WVCs and works consistently for the C&Ku wind retrieval.
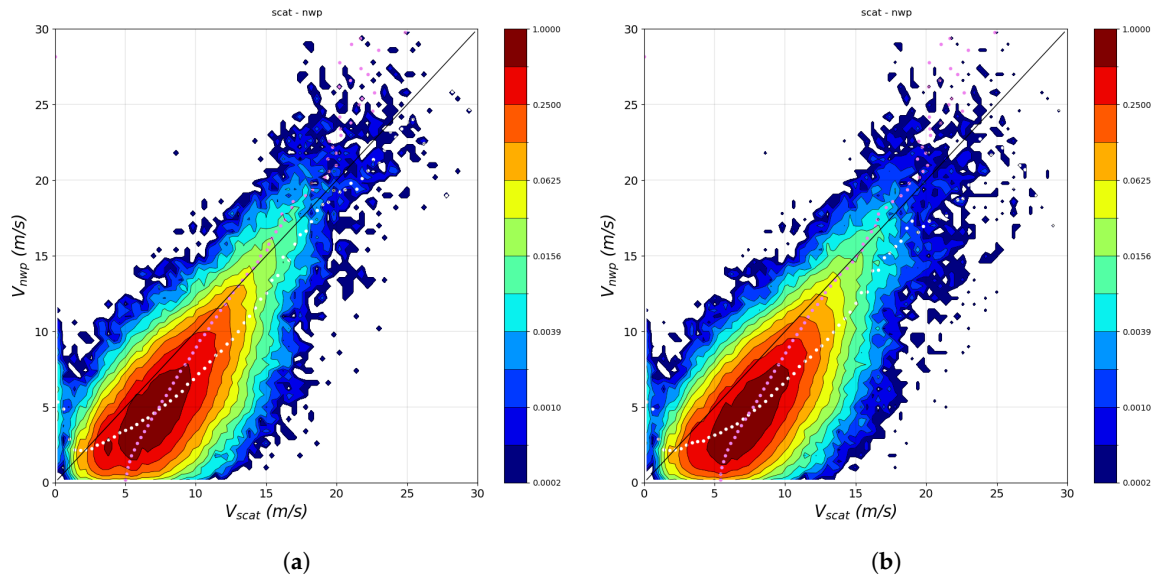

(**a**)   (**b**)

Figure 12. Contour plots of rejected winds against NWP winds, data from August 2023 to March 2024, latitude [-20°, 20°]: (**a**) rejected winds using R_n QC; (**b**) rejected winds using $R_n J$ QC.

Table 4. Wind statistics (C&Ku) for R_n QC and R_nJ QC against NWP winds, tropical latitude region [-20°, 20°], data from August 2023 to March 2024.

	QC method	Speed bias (m/s)	SDD of u (m/s)	SDD of v (m/s)
Rejected winds	R_n	2.301	2.24	2.35
	R_nJ	2.690	2.42	2.50
Accepted Winds	R_n	0.120	1.14	1.22
	R_nJ	0.103	1.12	1.20

Table 5. Wind statistics (C&Ku) for R_n QC and R_nJ QC against WindRAD C-band winds, tropical latitude region [-20°, 20°], data from August 2023 to March 2024.

	QC method	Speed bias (m/s)	SDD of u (m/s)	SDD of v (m/s)
Rejected winds	R_n	1.375	2.82	2.40
	R_nJ	1.293	2.97	2.60
Accepted Winds	R_n	0.359	1.27	1.22
	R_nJ	0.355	1.25	1.21

5. Conclusions

WindRAD is a dual-frequency rotating-fan-beam scatterometer with C-band and Ku-band antennas. C-band measurements are only little influenced by rain, whereas Ku-band measurements are very sensitive to heavy rain because of their shorter wavelength. In this article, the QC in association with rain contamination for Ku-band and C&Ku wind retrievals has been thoroughly investigated, focusing on the tropical region. The normalized MLE residual R_n and the combined method R_nJ (R_n and J_{OSS}) are adapted to the WindRAD measurements. The R_n threshold is a trade-off between a high rejection rate of low quality winds and a low rejection rate of good quality winds. J_{OSS} considers spatial consistency, and it is an excellent complementary indicator in detecting rainy WVCs [17]. The R_nJ is a combination of R_n and J_{OSS} that makes use of both the local information (MLE) and the spatial consistency (J_{OSS}).

For Ku-band wind retrieval, first an optimal R_n threshold is set and then the R_n QC is combined with J_{OSS} QC. An additional 0.41% of WVCs are rejected when R_nJ QC is used. With more rejected winds, the statistics of rejected wind are worse than the results with R_n QC, indicating the more rejected winds are most likely rain-contaminated. The statistics of accepted winds are all slightly better than with R_n QC. Moreover, the number of accepted WVCs with high rain rate (> 7 mm/hr) is reduced by half for R_nJ QC, as compared to R_n QC. In conclusion, the combined R_nJ QC method can distinguish rain-contaminated WVCs better than the R_n QC method.

An important opportunity for the C&Ku wind retrieval is to use the Ku-based R_n instead of the total (C and Ku) R_n. The Ku-based R_n results and the total R_n results are compared for the same rejection rate of 0.7%. The rejected winds speed contour plot against NWP winds has a larger deviation from the diagonal for the Ku-based R_n than for the total R_n. The reason for this is that rain does not influence the C-band observations to any substantial extent, and hence, the C-band measurement noise contribution to R_n may lead to false alarms in rain detection. Thus, the Ku-based R_n QC is more effective than the total R_n QC to identify rainy WVCs.

1.11% of the C&Ku wind retrievals are rejected by Ku-based R_n QC, which is reduced by about half compared to the Ku-band-only retrievals. At the same time and with the reduced rejection rate, the statistics of the accepted and rejected winds do not differ much from those using Ku-band-only retrievals. When using Ku-based R_n and looking at the WVCs with a high rain rate of over 7 mm/hr, three times more accepted winds are retrieved using C&Ku than using Ku-band-only. This indicates that combining the C-band with the Ku-band suppresses the rain effect in the wind retrieval and hence achieves good-quality winds with fewer rejected WVCs. The Ku-based R_n and R_nJ for C&Ku

retrievals are also compared. An additional 0.42% of WVCs are rejected by the Ku-based R_nJ. Like for the Ku-band-only retrieval, the statistics of rejected winds are worse than the results with R_n QC, and at the same time, the statistics of accepted winds are slightly improved compared to the result with R_n QC. Therefore, the Ku-based R_nJ can accurately exclude more rainy WVCs and its performance characteristics are consistent with the Ku-band-only wind retrieval results.

Above all, the R_nJ is an optimal QC method to detect rain contamination for wind retrievals where Ku-band observations are used. The Ku-based R_n is the key to improving QC for C&Ku wind retrieval. Adding the C-band observations to the wind retrieval suppresses the rain effect, and the same QC skill (in terms of accepted wind statistics) can be achieved with fewer rejected WVCs.

The very different rain effect for C-band and Ku-band may furthermore be exploited in the future for rain correction and as such further improve the quality of the WindRAD ocean surface vector winds in rainy areas. In addition, WindRAD may have a good capability to measure rain rates, which may be exploited in such future work.

Abbreviations

The following abbreviations are used in this manuscript:

ASCAT	Advanced Scatterometer
ECMWF	European Centre for Medium-Range Weather Forecasts
FY-3E	Fengyun-3E
GMF	Geophysical Model Function
GPM	Global Precipitation Measurement
HOC	Higher Order Calibration
HY	Hai Yang
KNMI	Royal Netherlands Meteorological Institute
MLE	Maximal Likelihood Estimation
NOCant	NWP Ocean Calibration as a function of incidence angle and relative antenna angle
NWP	Numerical Weather Prediction
OSI SAF	Ocean and Sea Ice Satellite Application Facility
PDF	Probability Density Function
QC	Quality Control
SST	Sea Surface Temperature
SDD	Standard Deviation Difference
WindRAD	Wind Radar
WVC	Wind Vector Cell
2DVAR	2-D Variational Ambiguity Removal
3IMERG	Level-3 Integrated Multi-satellitE Retrievals for GPM

References

1.   Jiang, X.; Lin, M.; Liu, J.; Zhang, Y.; Xie, X.; Peng, H.; Zhou, W. The HY-2 satellite and its preliminary assessment. *International Journal of Digital Earth* **2012**, *5*, 266–281. doi:10.1080/17538947.2012.658685.

2.   Gelsthorpe, R.V.; Schied, E.; Wilson, J.J.W. ASCAT - Metop's advanced scatterometer. *ESA BULLETIN-EUROPEAN SPACE AGENCY* **2000**.

3.   Li, Z.; Verhoef, A.; Stoffelen, A.; Shang, J.; Dou, F. First Results from the WindRAD Scatterometer on Board FY-3E: Data Analysis, Calibration and Wind Retrieval Evaluation. *Remote Sensing* **2023**, *15*, 2087. doi:10.3390/15082087.

4.   Li, Z.; Stoffelen, A.; Verhoef, A.; Wang, Z.; Shang, J.; Yin, H. Higher-order calibration on WindRAD (Wind Radar) scatterometer winds. *Atmospheric Measurement Techniques* **2023**, *16*, 4769–4783. doi:10.5194/amt-16-4769-2023.

5.   Chi, C.Y.; Li, F.K. A comparative study of several wind estimation algorithms for spaceborne scatterometers. *IEEE Transactions on Geoscience and Remote Sensing* **1988**, *26*, 115–121. doi:10.1109/36.3011.

6.   Pierson, W.J. Probabilities and statistics for backscatter estimates obtained by a scatterometer. *Journal of Geophysical Research* **1989**. doi:10.1029/JC094iC07p09743.

7.   Portabella, M.; Stoffelen, A. Characterization of Residual Information for SeaWinds Quality Control. *IEEE Trans. Geosci. Rem. Sens* **2002**, *40*, 2747–2759.

8.   Cornford, D.; Csató, L.; Evans, D.J.; Opper, M. Bayesian Analysis of the Scatterometer Wind Retrieval Inverse Problem: Some New Approaches. *Journal of the Royal Statistical Society. Series B (Statistical Methodology)* **2004**, *66*, 609–652.

9.   Stoffelen, A.; Portabella, M. On Bayesian Scatterometer Wind Inversion. *IEEE Transactions on Geoscience and Remote Sensing* **2006**, *44*, 1–11. doi:10.1109/TGRS.2005.862502.

10. Isaksen, L.; Stoffelen, A. ERS scatterometer wind data impact on ECMWF's tropical cyclone forecasts. *IEEE Transactions on Geoscience and Remote Sensing* **2000**, *38*, 1885–1892. doi:10.1109/36.851771.

11. Atlas, R.; Hoffman, R.N.; Leidner, S.M.; Sienkiewicz, J.; Yu, T.W.; Bloom, S.C.; Brin, E.; Ardizzone, J.; Terry, J.; Bungatoand, D.; Jusem, J.C. The Effects of Marine Winds from Scatterometer Data on Weather Analysis and Forecasting. *Bull. Amer. Meteor. Soc.* **2001**, *82*, 1965–1990. doi:https://doi.org/10.1175/1520-0477(2001)082<1965:TEOMWF>2.3.CO;2.

12. Singh, R.; Kumar, P.; Pal, P.K. Assimilation of oceansat-2-scatterometer-derived surface winds in the weather research and forecasting model. *IEEE Transactions on Geoscience and Remote Sensing* **2012**. doi:10.1109/TGRS.2011.2164410.

13. Belmonte Rivas, M.; Stoffelen, A. Characterizing ERA-Interim and ERA5 surface wind biases using ASCAT. *Ocean Science* **2019**, *15*, 831–852. doi:10.5194/os-15-831-2019.

14. Trindade, A.; Portabella, M.; Stoffelen, A.; Lin, W.; Verhoef, A. ERAstar: A High-Resolution Ocean Forcing Product. *IEEE Transactions on Geoscience and Remote Sensing* **2020**, *58*, 1337–1347. https://doi.org/10.1109/TGRS.2019.2946019.

15. Van de Hulst, H.C. *Light scattering by small particles*; John Wiley and Sons: New York, 1958.

16. Portabella, M.; Stoffelen, A. Rain Detection and Quality Control of SeaWinds. *Journal of Atmospheric and Oceanic Technology* **2001**, *18*, 1171–1183. https://doi.org/https://doi.org/10.1175/1520-0426(2001)018<1171:RDAQCO>2.0.CO;2.

17. Xu, X.; Stoffelen, A. Improved Rain Screening for Ku-Band Wind Scatterometry. *IEEE Transactions on Geoscience and Remote Sensing* **2020**, *58*, 2494–2503. doi:10.1109/TGRS.2019.2951726.

18. Zhao, K.; Stoffelen, A.; Verspeek, J.; Verhoef, A.; Zhao, C. Bayesian Algorithm for Rain Detection in Ku-Band Scatterometer Data. *IEEE Transactions on Geoscience and Remote Sensing* **2023**, *61*. https://doi.org/10.1109/TGRS.2023.3264245.

19. BLIVEN, L.F.; GIOVANANGELI, J.P. An experimental study of microwave scattering from rain- and wind-roughened seas. *International Journal of Remote Sensing* **1993**, *14*, 855–869. doi:10.1080/01431169308904382.

20. Craeye, C.; Schlüssel, P. Rainfall on the sea: Surface Renewals and Damping. *Boundary-Layer Meteorol.* **1998**, *89*, 349–355.

21. Tournadre, J. Impact of rain cell on scatterometer data: 1. Theory and modeling. *Journal of Geophysical Research* **2003**. doi:10.1029/2002JC001428.

22.   Stoffelen, A.; Anderson, D. Scatterometer data interpretation: Measurement space and inversion. *Journal of Atmospheric and Oceanic Technology* **1997**, *14*, 1298–1313. https://doi.org/10.1175/1520-0426(1997)014<1298:SDIMSA>2.0.CO;2.

23.   Figa, J.; Stoffelen, A. On the assimilation of Ku-band scatterometer winds for weather analysis and forecasting. *IEEE Transactions on Geoscience and Remote Sensing* **2000**, *38*, 1893–1920. doi:doi: 10.1109/36.851772.

24.   Li, Z.; Verhoef, A.; Stoffelen, A.; Verhoef, A.; Verhoef, A. CWDP L2A processor Specification and User Manual. Technical report, KNMI, de Bilt, the Netherlands, 2019.

25.   Xu, X.; Stoffelen, A.; Lin, W.; Dong, X. Rain False-Alarm-Rate Reduction for CSCAT. *IEEE Geoscience and Remote Sensing Letters* **2022**, *19*. doi:10.1109/LGRS.2020.3039622.

26.   Bolvin, D.T.; Joyce, R.; Nelkin, E.J.; Tan, J.; Braithwaite, D.; Hsu, K.; Kelley, O.A.; Nguyen, P.; Sorooshian, S.; Watters, D.C.; West, B.J.; Xie, P. Algorithm Theoretical Basis Document (ATBD) NASA Global Precipitation Measurement (GPM) Integrated Multi-satellitE Retrievals for GPM (IMERG) Version 07. Technical report, NASA, Greenbelt, 2023.

27.   De Kloe, J.; Stoffelen, A.; Verhoef, A. Improved Use of Scatterometer Measurements by Using Stress-Equivalent Reference Winds. *IEEE Journal of Selected Topics in Applied Earth Observations and Remote Sensing* **2017**, *10*. doi:10.1109/JSTARS.2017.2685242.

28.   Vogelzang, J.; Stoffelen, A. On the Accuracy and Consistency of Quintuple Collocation Analysis of In Situ, Scatterometer, and NWP Winds. *Remote Sensing* **2022**, *14*. doi:10.3390/rs14184552.

29.   Vogelzang, J. Two-dimensional variational ambiguity removal (2DVAR). Technical report, KNMI, de Bilt, the Netherlands, 2013.

30.   Verhoef, A.; Stoffelen, A. Advances in Ku-band scatterometer Quality Control. Technical report, 2021.